Marine Geology 402 (2018) 5–16

Contents lists available at ScienceDirect

Marine Geology

journal homepage: www.elsevier.com/locate/margo

Baffin Bay paleoenvironments in the LGM and HS1: Resolving the ice-shelf question

Anne E. Jennings[a,*], John T. Andrews[a], Colm Ó Cofaigh[b], Guillaume St-Onge[c], Simon Belt[d], Patricia Cabedo-Sanz[d], Christof Pearce[e,f], Claude Hillaire-Marcel[g], D. Calvin Campbell[h]

[a] INSTAAR University of Colorado, Campus Box 450, Boulder, CO 80309-0450, USA
[b] Department of Geography, Durham University, South Road, Durham DH1 3LE, United Kingdom
[c] Institut des Sciences de la mer de Rimouski (ISMER), Université du Québec à Rimouski and GEOTOP Rimouski, Québec S5L 3A1, Canada
[d] School of Geography, Earth and Environmental Sciences, University of Plymouth, Plymouth PL4 8AA, United Kingdom
[e] Department of Geological Sciences and Bolin Centre for Climate Research, Stockholm University, Svante Arrhenius väg 8, SE-106 91 Stockholm, Sweden
[f] Department of Geoscience and Arctic Research Centre, Aarhus University, Hoegh Guldbergs gade 2, 8000 Aarhus, Denmark
[g] Université du Québec a Montréal, Centre GEOTOP CP 8888, succ. Centre-Ville, Montréal H3C 3P8, Québec, Canada
[h] Geological Survey of Canada-Atlantic, Natural Resources Canada, Dartmouth, Nova Scotia, Canada

ARTICLE INFO

Keywords:
Greenland Ice Sheet
Baffin Bay
Paleoceanography
Ice shelf
Foraminifera
Heinrich Stadial 1

ABSTRACT

Core HU2008029-12PC from the Disko trough mouth fan on the central West Greenland continental slope is used to test whether an ice shelf covered Baffin Bay during the Last Glacial Maximum (LGM) and at the onset of the deglaciation. We use benthic and planktic foraminiferal assemblages, stable isotope analysis of planktic forams, algal biomarkers, ice-rafted detritus (IRD), lithofacies characteristics defined from CT scans, and quantitative mineralogy to reconstruct paleoceanographic conditions, sediment processes and sediment provenance. The chronology is based on radiocarbon dates on planktic foraminifers using a ΔR of 140 ± 30 ^{14}C years, supplemented by the varying reservoir estimates of Stern and Lisiecki (2013) that provide an envelope of potential ages. HU2008029-12PC is bioturbated throughout. Sediments between the core base at 11.3 m and 4.6 m (LGM through HS1) comprise thin turbidites, plumites and hemipelagic sediments with Greenlandic provenance consistent with processes active at the Greenland Ice Sheet margin grounded at or near the shelf edge. Abundance spikes of planktic forams coincide with elevated abundance of benthic forams in assemblages indicative of chilled Atlantic Water, meltwater and intermittent marine productivity. IRD and IP_{25} are rare in this interval, but brassicasterol, an indicator of marine productivity reaches and sustains low levels during the LGM. These biological characteristics are consistent with a sea-ice covered ocean experiencing periods of more open water such as leads or polynyas in the sea ice cover, with chilled Atlantic Water at depth, rather than full ice-shelf cover. They do not support the existence of a full Baffin Bay ice shelf cover extending from grounded ice on the Davis Strait. Initial ice retreat from the West Greenland margin is manifested by a pronounced lithofacies shift to bioturbated, diatomaceous mud with rare IRD of Greenlandic origin at 467 cm (16.2 cal ka BP; ΔR = 140 yrs) within HS1. A spike in foraminiferal abundance and ocean warmth indicator benthic forams precedes the initial ice retreat from the shelf edge. At the end of HS1, IP_{25}, brassicasterol and benthic forams indicative of sea-ice edge productivity increase, indicating warming interstadial conditions. Within the Bølling/Allerød interstadial a strong rise in IP_{25} content and IRD spikes rich in detrital carbonate from northern Baffin Bay indicate that northern Baffin Bay ice streams were retreating and provides evidence for increased open water, advection of Atlantic Water in the West Greenland Current, and formation of an IRD belt along the W. Greenland margin.

1. Introduction

Last Glacial Maximum (LGM) climatic and oceanic conditions in Baffin Bay are currently poorly known, but according to the temperature reconstructions from the Greenland Ice Sheet borehole (Dahl-Jensen and Al, 1998) and ice-core data (Buizert et al., 2014), summit temperatures were ~20 °C colder than present. Applying this temperature difference down to sea level using the adiabatic lapse rate,

* Corresponding author.
E-mail address: anne.jennings@colorado.edu (A.E. Jennings).

http://dx.doi.org/10.1016/j.margeo.2017.09.002
Received 28 April 2017; Received in revised form 15 August 2017; Accepted 5 September 2017
Available online 06 September 2017

suggests that the annual temperature at the surface of Baffin Bay adjacent to Baffin Island would approach − 36 °C. Such cold temperatures support the argument that cold-based ice covered the forelands of eastern Baffin Island (Briner et al., 2003) with "Antarctic-like" conditions across Baffin Bay, which would also suggest that Baffin Bay was covered in perennial sea ice. At the LGM, confluent, Innuitian (IIS), Laurentide (LIS) and Greenland (GIS) ice sheets (England et al., 2006) blocked the channels that connect Baffin Bay to the Arctic Ocean (Dyke et al., 2002) and terminated in northern Baffin Bay as large ice streams (Li et al., 2011; Blake, 1977). The Greenland Ice Sheet reached the continental shelf edge via large ice streams off west Greenland (Ó Cofaigh et al., 2013a; Jennings et al., 2017; Slabon et al., 2016; Sheldon et al., 2016; Dowdeswell et al., 2014), but the outer limits of the ice on the Baffin shelf are not known.

On the basis of modeling, it has been proposed that Baffin Bay was blocked at its southern end by an ice shelf extension of the Hudson Strait ice stream that grounded across Davis Strait to reach southern Greenland, thus sealing Baffin Bay from the Labrador Sea (Hulbe, 1997; Álvarez-Solas et al., 2010; Marcott et al., 2011). This ice shelf was the starting point for modeling the processes that produce Heinrich events (Hulbe, 1997; Álvarez-Solas et al., 2010; Marcott et al., 2011), but physical evidence for it has not been recovered. An ice shelf of this scale would have environmental consequences that should be recorded in Baffin Bay sediments. Firstly, grounding of a Labrador Sea ice shelf along Davis Strait would prevent seawater exchange between Baffin Bay and the Labrador Sea, excluding advection of organic matter into Baffin Bay. It also would shut down in situ primary marine productivity in Baffin Bay so that planktic and benthic organisms, their biomarkers, and bioturbation would be absent in the sediment. Secondly, ice shelves and even extensive sea-ice cover are known to restrict the movement and export of icebergs (Reeh et al., 2001; Domack and Harris, 1998). Thus iceberg rafting and mixing of sediments of various provenances in Baffin Bay would be reduced. Using these concepts, we test the LGM Baffin Bay ice-shelf hypothesis by studying the sedimentological and biological characteristics of sediments in HU2008029-12PC from the continental slope off western Greenland, a core that extends from the LGM into the Younger Dryas (YD) and that recorded retreat of the Greenland Ice Sheet during deglaciation (Jennings et al., 2017).

2. Setting of core HU2008029-12PC

Detailed studies of LGM and deglacial environments in Baffin Bay have been hampered by relatively slow sediment accumulation rates and poor calcium carbonate preservation (cf. Aksu, 1985; de Vernal et al., 1992; Simon et al., 2012). HU2008029-12PC (hereafter called 12PC) was raised from the northern side of the Disko trough mouth fan (TMF) from acoustically stratified sediments with continuous parallel reflections on the eastern side of Baffin Bay (68°13.69′ N; 57°37.08′ W; 1475 m water depth; Campbell and de Vernal, 2009) (Figs. 1 and 2). This site on the trough mouth fan has higher sediment accumulation than sites in the deep basin of Baffin Bay that have variable sedimentation rates that range between 3 and 35 cm/ka (Andrews et al., 1998; Hillaire-Marcel et al., 1989; Hillaire-Marcel and de Vernal, 2008; Simon et al., 2012, 2014) (Fig. 1).

The Disko TMF was built throughout the Quaternary by rapid sediment deposition in front of the fast flowing Disko ice stream (Fig. 1) when the GIS margin was extended on the shelf, and from hemipelagic sedimentation during and after ice retreat (Ó Cofaigh et al., 2013a, 2013b; Jennings et al., 2017; Hofmann et al., 2016). An ice sheet grounded at or near the shelf edge delivers abundant sediments directly to the continental slope in the form of sediment gravity flows, including turbidity currents that form graded sand layers, stratified sand/silt beds, and glacigenic debris flows (Ó Cofaigh et al., 2013a, 2013b; Lucci and Rebesco, 2007). Turbid meltwater plumes released from the ice front produce plumites, which are finer grained than the turbidites as the sand is dropped near the ice front and the silt and clay continue

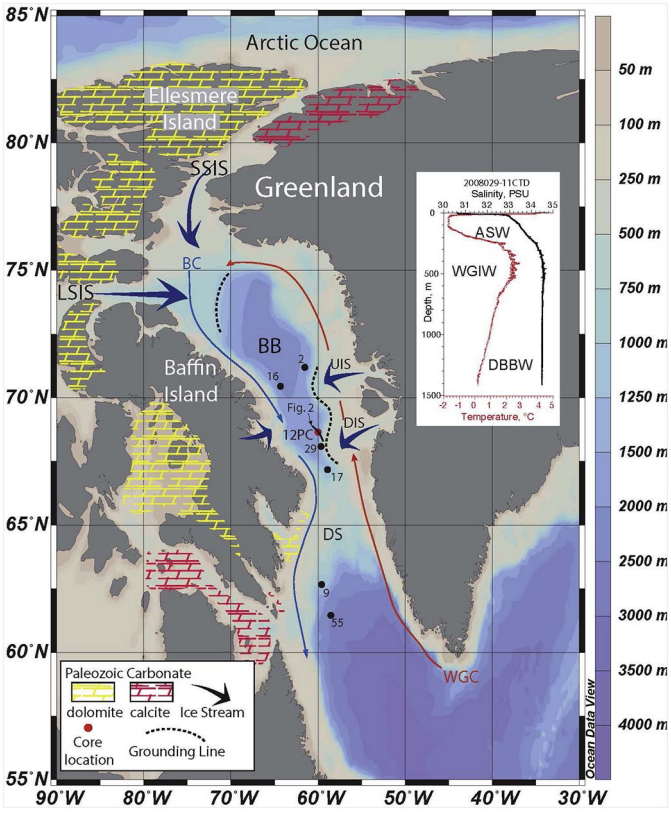

Fig. 1. Bathymetric map centered on Baffin Bay (BB) showing the location of core HU2008029-12PC (12PC) and other cores mentioned in the text, the distribution of Paleozoic carbonate bedrock, mapped ice margin positions in northern Baffin Bay (Li et al., 2011) and central west Greenland (Ó Cofaigh et al., 2013a) and major ice streams. UIS = Uummannaq ice stream; DIS = Disko ice stream; SSIS = Smith Sound ice stream; LSIS = Lancaster Sound ice stream. Northward flowing West Greenland Current (WGC) is shown as the thin red line and the southward flowing Baffin Current (BC) is shown as a thin blue line. The position of the acoustic profile in Fig. 2 is shown as a black line. HU2008029-016PC = 16; HE006-4-2PC = 2; JR175-VC29 = 29; HU77029-017PC = 17; HU75009-IV-055PC = 55 and HU87033-009 LCF = 9. Inset plot shows the salinity and temperature against water depth at from the same location as 2008029-12PC. ASW = Arctic Surface Water; WGIW = West Greenland Intermediate Water; DBBW = Deep Baffin Bay Water. (For interpretation of the references to colour in this figure legend, the reader is referred to the web version of this article.)

offshore in suspension (Hesse et al., 1997; Lucci and Rebesco, 2007). Depending on sea surface conditions such as perennial sea ice and/or ice shelves, icebergs would also deliver sediment to the slope as they melted during their transit in Baffin Bay (Andrews et al., 1998, 2014; Jennings et al., 2014; Simon et al., 2012, 2014, 2016; Sheldon et al., 2016).

The modern sea ice edge extends southeast to northwest within Baffin Bay and sea ice cover is greater in the western than in the eastern half due to the influence of the relatively warm and saline West Greenland Current that enters Baffin Bay from the southeast (Tang et al., 2004; Münchow et al., 2015) (Fig. 1). The boundary between lower salinity, sea-ice bearing, Arctic Surface Water (ASW) that passes from the Arctic Ocean through the channels of the Canadian Arctic Archipelago into Baffin Bay and Atlantic Waters of the West Greenland Current (WGC) moving northward along West Greenland is oriented NE-SW and migrates through the year. The relatively warm, saline Atlantic Water submerges beneath the ASW (Buch, 2000a, 2000b) and forms the West Greenland Intermediate Water (WGIW) (Fig. 1 inset) (Tang et al., 2004). During the LGM, however, the circulation regime in Baffin Bay would have been different because the southward flow of ASW into Baffin Bay was blocked by confluent ice sheets grounded in the channels of the Canadian Arctic Archipelago until the early Holocene (England, 1999; Zreda et al., 1999; Jennings et al., 2011;

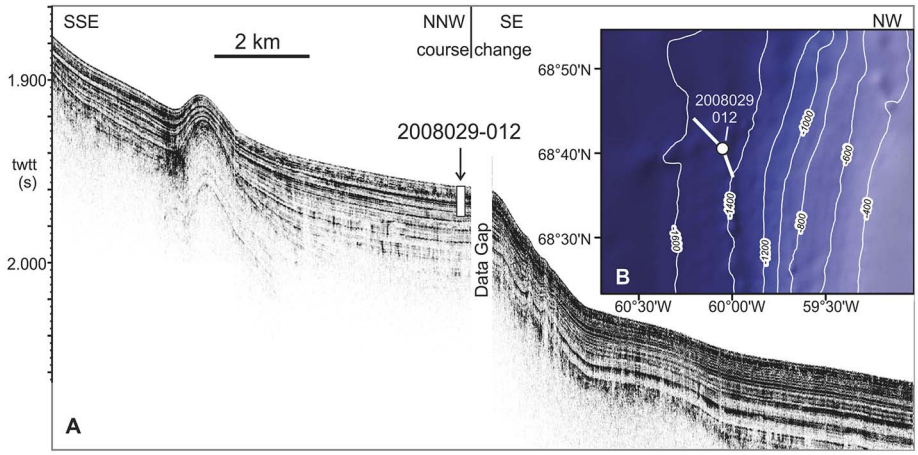

Fig. 2. A. 3.5 kHz sub-bottom profile over the site of 2008029-12PC demonstrationg the acoustically-stratified character of the seabed in the area. B. A zoom in map of the 3.5 kKz sub-bottom profile and the core location shown in Fig. 1. The bathymetry is from GEBCO.

Piénkowski et al., 2012). Today, warm Atlantic Water carried in the WGC accesses the GIS margins via cross shelf troughs and fjords, where the ice sheet terminates in the sea (Holland et al., 2008) and promotes basal melting (Straneo et al., 2012). WGC Atlantic Water flow was initiated as early as 14.4 cal ka BP off central West Greenland and is implicated in Greenland Ice Sheet retreat from the LGM position at the shelf edge (cf. Knutz et al., 2011; Sheldon et al., 2016; Jennings et al., 2017).

3. Methods

3.1. Age model

The age model for 12PC is based on 7 radiocarbon dates between 201 and 860 cm on the arctic planktic foraminifer, *Neogloboquadrina pachyderma* (sensu Darling et al., 2006). The dates were previously published in Jennings et al. (2017) (Table 1). Radiocarbon dates were calibrated using the Marine13 curve (Reimer et al., 2013). OxCal version 4.2.4 (Ramsey and Lee, 2013) was used to compute an age/depth model (Fig. 3). An age reversal in the upper 110 cm of the core limited the chronology to the interval from 200 cm to the base of the core (1130 cm). The age of the core base is assumed to be no older than 26.5 ka BP, the beginning of the LGM (Clark et al., 2009). This assumed basal age results in a large uncertainty in the modeled age of the base of the core (24 to 28 cal ka BP). Given this basal age, we might expect to record Baffin Bay Detrital Carbonate (BBDC) event BBDC3 that is found in central Baffin Bay from c. 23.5 to 25 cal ka BP (Simon et al., 2016). A single data point with 20% NBB source at 21.5 cal ka BP may represent BBDC2 (21 cal ka BP; Simon et al., 2016) although it is not associated with a coarse clast-rich interval as would be expected if it represented a BBDC event (Andrews et al., 1998; Simon et al., 2012; Jackson et al., 2017) (Fig. 3). The lack of an interval of high NBB and IRD below 467 cm (16.2 cal ka BP) in 12PC indicates that BBDC2 and BBDC3 were not recovered in 12PC. Either these two events were not deposited basin wide or the basal age of 12PC is younger than the 21 ka BP age of BBDC2. Given that the deepest radiocarbon age in 12PC is 21.8 cal ka BP (ΔR = 140 years) and there are 3 m of sediment below this depth in the core, we suggest it is more likely that BBDC2 and 3 were not deposited basin wide. Without additional information we continue with the assumption that the core base is no older than the beginning of the global LGM of 26.5 ka BP (Clark et al., 2009).

We initially built the age model assuming a marine reservoir offset (ΔR) of 140 ± 30 years based on recent work in Disko Bugt (Lloyd et al., 2011), for consistency with other central West Greenland sediment core records (cf Jennings et al., 2014, 2017; Jackson et al., 2017; Hogan et al., 2016; Sheldon et al., 2016), and we note that prior to 2011, many publications used a ΔR = 0 years (Andrews et al., 1998; Knudsen et al., 2008). However, recognizing that the marine reservoir offset could be large and variable over the time interval of 12PC and because this core extends into the LGM, defined here as beginning at 26.5 ka (Clark et al., 2009) and ending at the beginning of the Oldest Dryas period, 18 ka BP (Buizert et al., 2014), we used the variable North Atlantic R values in Stern and Lisiecki (2013) to provide an envelope of calibrated age so that we could consider the correlations of boundaries and conditions recorded in the core with established climatic intervals (Fig. 3f). To accomplish this we first calibrated each date with $\Delta R = 0$ ^{14}C years, which provides the maximum age. We then used the $\Delta R = 0$ ages to identify the appropriate 500 year bin of maximum, average and minimum R values from Table S1 of Stern and Lisiecki (2013) and calibrated each of the dates using these three R-values. The resulting envelope of ages, from $\Delta R = 0$ to the maximum Stern and Lisiecki, 2013 R-value, illustrates how the choice of ΔR affects correlation of boundaries in the core with climate intervals from LGM through the YD (Fig. 3f; Table 1). Regardless, these results confirm that the core contains LGM and Heinrich Stadial 1 (aka Oldest Dryas) sediments, a key requirement for testing the ice shelf model (Hulbe, 1997; Álvarez-Solas et al., 2010; Marcott et al., 2011).

3.2. Foraminiferal analyses

One-cm wide samples were weighed wet and sieved on a 63-μm screen. Material > 63 μm was kept wet in a storage solution of 70% distilled water and 30% ethanol with baking soda as a buffer. Foraminifera were counted wet to prevent destruction of fragile tests that disintegrate under the stress of drying. A wet splitter was used when necessary to achieve a count of 200–300 benthic formaminifers and as many planktic foraminifers as were in the benthic split. In most cases the full sample was counted. Equivalent dry weights of the foram samples were estimated from sedimentology samples from the same depths that had both wet and dry weights, allowing foraminifera/g sediment to be calculated.

3.3. Stable isotope analyses

Stable oxygen and carbon isotopes were measured on the planktic foram species *Neogloboquadrina pachyderma* picked from the 150–250 μm size fraction in 41 samples; results from 3 samples were rejected because they yielded a low signal. Samples > 100 μg have standard deviations of 0.01 and 0.03‰ for $\delta^{13}C$ and $\delta^{18}O$ respectively. Samples weighing < 100 μg are reported with a standard deviation of 0.06‰ for $\delta^{13}C$, and an error of ± 0.2‰ for $\delta^{18}O$. The oxygen isotope values are expressed as ‰ vs VPDB. Between 1050 and 857 cm all samples were of small weight but otherwise seemed reliable. Measurements were made on a Micromass IsoprimeTM dual inlet coupled to a MulticarbTM system at the Light Stable Isotope Geochemistry Laboratory at the University of Montréal - UQAM.

Table 1
Radiocarbon ages and their calibrations with varying ΔR.

HU2008029-12PC					Calibrated							
Date	Depth	14C	error	ΔR	Date (14C age, error)	1sigma from	1sigma to	2sigma from	2sigma to	Mean	Error	Median
CURL14065	201.5	10,760	35	0	CURL14065 with DR = 0 (10,760,35)	12,306	12,075	12,430	12,028	12,215	109	12,207
CURL14065	201.5	10,760	35	140	CURL14065 with DR = 140 (10,620,35)	12,026	11,865	12,100	11,755	11,937	86	11,943
CURL14065	201.5	10,760	35	470	CURL14065 with min DR = 470 (10,290,35)	11,317	11,210	11,432	11,161	11,282	70	11,270
CURL14065	201.5	10,760	35	900	CURL14065 with mean DR = 900 (9860,35)	10,868	10,706	10,972	10,667	10,805	79	10,796
CURL14065	201.5	10,760	35	1340	CURL14065 with max DR = 1340 (9420,35)	10,291	10,196	10,373	10,176	10,260	51	10,250
AA90386	251.5	12,666	61	0	AA90386 with DR = 0 (12,666,61)	14,279	14,051	14,542	13,964	14,208	142	14,180
AA90386	251.5	12,666	61	140	AA90386 with DR = 140 (12,526,61)	14,095	13,926	14,165	13,840	14,007	83	14,009
AA90386	251.5	12,666	61	380	AA90386 with min DR = 380 (12,286,61)	13,845	13,665	13,930	13,555	13,748	91	13,751
AA90386	251.5	12,666	61	630	AA90386 with mean DR = 630 (12,036,61)	13,552	13,392	13,657	13,332	13,484	81	13,478
AA90386	251.5	12,666	61	900	AA90386 with max DR = 900 (11,766,61)	13,312	13,180	13,375	13,114	13,246	66	13,246
CURL16671	469.5	14,030	40	0	CURL16671 with DR = 0 (14,030,40)	16,511	16,309	16,632	16,233	16,423	102	16,416
CURL16671	469.5	14,030	40	140	CURL16671 with DR = 140 (13,890,40)	16,311	16,144	16,424	16,045	16,232	90	16,230
CURL16671	469.5	14,030	40	850	CURL16671 with min DR = 850 (13,180,40)	15,282	15,148	15,375	15,076	15,221	73	15,218
CURL16671	469.5	14,030	40	1260	CURL16671 with mean DR = 1260 (12,770,40)	14,507	14,193	14,701	14,136	14,398	155	14,378
CURL16671	469.5	14,030	40	1500	CURL16671 with max DR = 1500 (12,530,40)	14,086	13,947	14,143	13,873	14,011	68	14,014
CURL18165	571.5	15,150	60	0	CURL18165 with DR = 0 (15,150,60)	18,035	17,854	18,130	17,740	17,941	94	17,943
CURL18165	571.5	15,150	60	140	CURL18165 with DR = 140 (15,010,60)	17,887	17,687	17,973	17,598	17,785	97	17,786
CURL18165	571.5	15,150	60	500	CURL18165 with min DR = 500 (14,650,60)	17,465	17,236	17,549	17,125	17,345	110	17,349
CURL18165	571.5	15,150	60	1150	CURL18165 with mean DR = 1150 (14,000,60)	16,491	16,261	16,631	16,174	16,390	117	16,381
CURL18165	571.5	15,150	60	1750	CURL18165 with max DR = 1750 (13,400,60)	15,680	15,408	15,776	15,297	15,541	128	15,544
CURL14067	690.5	16,660	45	0	CURL14067 with DR = 0 (16,660,45)	19,698	19,528	19,832	19,467	19,631	91	19,621
CURL14067	690.5	16,660	45	140	CURL14067 with DR = 140 (16,520,45)	19,550	19,372	19,609	19,260	19,449	88	19,455
CURL14067	690.5	16,660	45	290	CURL14067 with min DR = 290 (16,370,45)	19,368	19,168	19,466	19,070	19,268	99	19,264
CURL14067	690.5	16,660	45	720	CURL14067 with mean DR = 720 (15,940,45)	18,850	18,739	18,905	18,674	18,791	57	18,793
CURL14067	690.5	16,660	45	1250	CURL14067 with max DR = 1250 (15,410,45)	18,328	18,149	18,395	18,039	18,226	90	18,234
CURL16663	780.5	16,600	50	0	CURL16663 with DR = 0 (16,600,50)	19,634	19,467	19,749	19,360	19,553	91	19,551
CURL16663	780.5	16,600	50	140	CURL16663 with DR = 140 (16,460,50)	19,480	19,283	19,560	19,203	19,380	93	19,382
CURL16663	780.5	16,600	50	290	CURL16663 with min DR = 290 (16,310,50)	19,257	19,061	19,385	18,986	19,177	99	19,173
CURL16663	780.5	16,600	50	720	CURL16663 with mean DR = 720 (15,880,50)	18,802	18,680	18,856	18,605	18,735	62	18,738
CURL16663	780.5	16,600	50	1250	CURL16663 with max DR = 1250 (15,350,50)	18,267	18,071	18,337	17,973	18,160	94	18,163
CURL18628	859.5	18,540	80	0	CURL18628 with DR = 0 (18,540,80)	22,113	21,850	22,271	21,751	21,993	131	21,985
CURL18628	859.5	18,540	80	140	CURL18628 with DR = 140 (18,400,80)	21,916	21,670	22,057	21,537	21,795	127	21,798
CURL18628	859.5	18,540	80	-50	CURL18628 with min DR = − 50 (18,590,80)	22,175	21,905	22,301	21,820	22,051	128	22,048
CURL18628	859.5	18,540	80	420	CURL18628 with mean DR = 420 (18,120,80)	21,594	21,299	21,746	21,137	21,442	149	21,444
CURL18628	859.5	18,540	80	1010	CURL18628 with max DR = 1010 (17,530,80)	20,772	20,537	20,913	20,434	20,662	119	20,657
Base of H1 ages from the Labrador Sea												
HU87033–009 LCF, 500–501 cm; Jennings et al. (1996)												
AA-9364		14,980	90	0	AA-9364 with DR = 0 (14,980,90)	17,878	17,633	17,984	17,515	17,752	120	17,753
AA-9364		14,980	90	140	AA-9364 with DR = 140 (14,840,90)	17,725	17,460	17,883	17,333	17,599	136	17,597
AA-9364		14,980	90	500	AA-9364 with min DR = 500 (14,480,90)	17,281	16,963	17,437	16,789	17,115	161	17,115
AA-9364		14,980	90	1150	AA-9364 with mean DR = 1150 (13,830,90)	16,288	16,021	16,449	15,861	16,155	140	16,154
AA-9364		14,980	90	1750	AA-9364 with max DR = 1750 (13,230,90)	15,443	15,143	15,656	15,041	15,318	155	15,302
HU75009-IV-055PC, 115–117 cm; Kaufman and Williams (1992)												
AA-5999		15,010	105	0	AA-5999 with DR = 0 (15,010,105)	17,916	17,650	18,037	17,513	17,780	133	17,781
AA-5999		15,010	105	140	AA-5999 with DR = 140 (14,870,105)	17,785	17,490	17,925	17,345	17,634	147	17,633
AA-5999		15,010	105	500	AA-5999 with min DR = 500 (14,510,105)	17,345	17,000	17,495	16,800	17,156	174	17,159
AA-5999		15,010	105	1150	AA-5999 with mean DR = 1150 (13,860,105)	16,345	16,032	16,538	15,875	16,200	163	16,195
AA-5999		15,010	105	1750	AA-5999 with max DR = 1750 (13,260,105)	15,528	15,180	15,733	15,060	15,367	174	15,356

3.4. CT scan

CT scanning of the half round core was performed at the sediment core laboratory at the University of Quebec at Rimouski. A CT number (a measure of sediment density) was extracted from the images. The CT scan image was used to determine lithofacies and boundaries, sedimentary structures, and to identify bioturbation, a key source of evidence for the presence of benthic organisms and a source of information about sedimentation rate variations between the radiocarbon dates (Wetzel, 1991). Counts of > 2 mm clasts interpreted as ice rafted detritus (IRD) were made from the CT images by counting in a 2 cm wide window across the core width continuously along the core length (Grobe, 1987).

3.5. Biomarkers: IP_{25} and brassicasterol

Biomarker analyses (IP_{25} and brassicasterol) were performed using methods described previously (Belt et al., 2012; Belt et al., 2015). Briefly, 9-octylheptadec-8-ene (9-OHD, 10 μL; 10 μg mL^{-1}) and 5α-androstan-3β-ol (10 μL; 10 μg mL^{-1}) were added to ca. 1–2 g of each freeze-dried sediment sample prior to extraction to permit quantification of IP_{25} and sterols, respectively. Samples were then extracted using dichloromethane/methanol (3 × 3 mL; 2:1 v/v) and ultrasonication. Following removal of the solvent from the combined extracts using nitrogen, the resulting total organic extracts (TOE) were purified using column chromatography (silica) with IP_{25} (hexane; 6 mL) and brassicasterol (20:80 methylacetate/hexane; 6 mL) collected as two single fractions. Non-polar lipid fractions were further separated into saturated and unsaturated hydrocarbons using glass pipettes containing silver ion solid phase extraction material (Supelco Discovery® Ag-Ion). Saturated hydrocarbons were eluted with hexane (1 mL), while unsaturated hydrocarbons (including IP_{25}) were eluted with acetone (2 mL). All fractions were dried under a stream of nitrogen.

Analysis of individual fractions was carried out using gas chromatography-mass spectrometry (GC-MS) with operating conditions as described previously (e.g. Belt et al., 2012; Brown and Belt, 2012). Sterols were derivatized (BSTFA; 50 μL; 70 °C; 1 h) prior to analysis by GC-MS. Mass spectrometric analysis was carried out in total ion current (TIC)

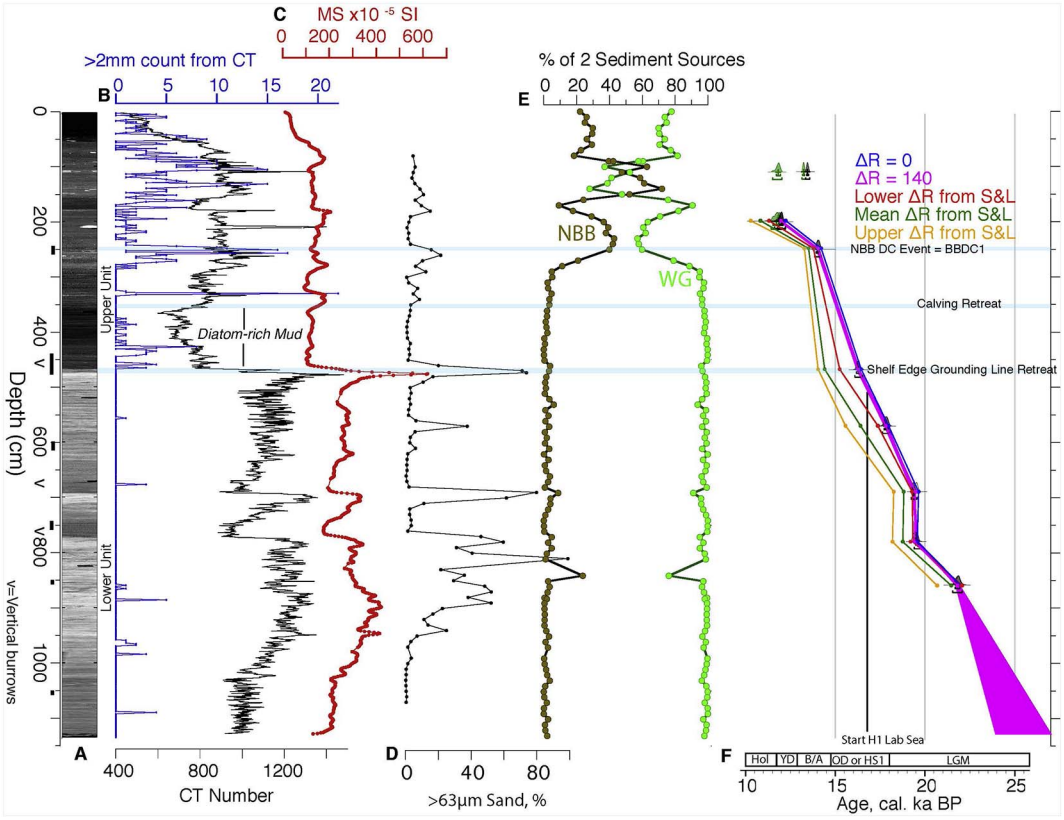

Fig. 3. Lithological proxies and age control for 2008029-12PC. A is the CT image against depth in the core. Black bars along depth axis show the locations of CT images shown in Fig. 4. 'V' denotes locations of vertical burrows. B. IRD counts (> 2 mm clasts) from CT scan in 2 cm increments. C. CT number, a measure of density derived from the CT image. D. Magnetic Susceptibility measure by multi sensor track (MST). E. Weight percentage of > 63 µm sand fraction from foraminiferal samples. F. Two-source provenance of minerals: Northern Baffin Bay (NBB, brown) vs. the local source, central west Greenland (green). F. Depth-Age model in pink (ΔR = 140 ± 30 yrs) showing 1σ and 2σ uncertainties of the model. Excluded from the model are benthic foraminiferal ages (green distributions) and outliers at 1 m. Age envelope for other potential ΔR calibrations are shown by blue (ΔR = 0); Red, green, orange = lower, mean, and upper ΔR values from Stern and Lisiecki (2013). Climate units are along the age scale. (For interpretation of the references to colour in this figure legend, the reader is referred to the web version of this article.)

and single-ion monitoring (SIM) modes. Individual lipids were identified on the basis of their characteristic GC retention indices and mass spectra obtained from standards. Quantification of IP_{25} was achieved by dividing its integrated GC-MS peak area by that of the internal standard (9-OHD) in SIM mode (both *m/z* 350) and normalizing this ratio using an instrumental response factor (obtained from laboratory standards of each analyte) and the mass of sediment (Belt et al., 2012). Analytical reproducibility (6%, n = 3) was monitored using a sediment with a known concentration of IP_{25}. Brassicasterol concentrations were obtained by comparison of their respective peak areas in SIM mode (brassicasterol, *m/z* 470) with those of the internal standard (*m/z* 333) and normalized as per IP_{25}.

3.6. Quantitative X-ray diffraction mineralogy

Quantitative X-ray diffraction (qXRD) analyses were used to identify shifts in sediment sources between 'local' West Greenland (WG) and 'distal' Northern Baffin Bay (NBB). Samples for qXRD analysis were taken at 10 to 20 cm intervals throughout the core. Sediment samples were freeze-dried and processed at INSTAAR using the method described by Eberl (2003) and Andrews and Eberl (2011). The qXRD samples were analysed on a Siemens D5000 XRD unit at a 0.02 2-θ step with a 2 s count; minerals were identified using the program RockJock v.6 (Eberl, 2003). The qXRD 2-source data to 17.5 cal ka BP is presented in Jennings et al. (2017). The determination of sediment provenance is based on the quantitative X-ray diffraction (qXRD) analysis of the < 2 mm surface and core sediments using the method outlined by Eberl (2003) and described in more detail for our area by (Andrews and Eberl, 2012; Andrews et al., 2014; Ó Cofaigh et al., 2013a; Simon et al., 2014). We use the Excel macro unmixing program "SedUnMix" (Eberl, 2003; Andrews and Eberl, 2012) to ascribe sediment mineral assemblages to probable source areas. In this present study we discriminated between two glacial derived sources; first a regional West Greenland source dominated by specific ranges in quartz, plagioclase, k-feldspars and other non-clay and clay minerals, versus a North Baffin Bay detrital carbonate source dominated by dolomite (Andrews et al., 2014; Ó Cofaigh et al., 2013a, 2013b; Jennings et al., 2017).

4. Results and interpretation

4.1. Lithofacies characteristics

There are two main lithofacies units defined by the sediment parameters in 12PC (Fig. 3). The boundary between the two units (Fig. 4b) is well expressed by an abrupt shift to lower CT# (Fig. 3A). This transition dates to 16.2 cal ka BP using ΔR = 140 years and has been interpreted to represent the retreat of the Greenland Ice Sheet from the shelf edge (Jennings et al., 2017). However, the full age-envelope ranges between 16.4 (ΔR = 0) to 14.0 (Max R) ka, or, late in Heinrich Stadial 1 to the end of the Bølling (Fig. 3f). Calibrated radiocarbon dates (Fig. 3F; ΔR = 140, pink) in the lower unit range from 21.8 to 16.2 cal ka BP. The lower three radiocarbon dates fall within the LGM regardless of the marine reservoir age selected (Fig. 3F). The radiocarbon date at 571.5 cm falls within Heinrich Stadial 1 regardless of the marine reservoir age (Fig. 3F).

The lower lithofacies unit, which represents the period when the ice

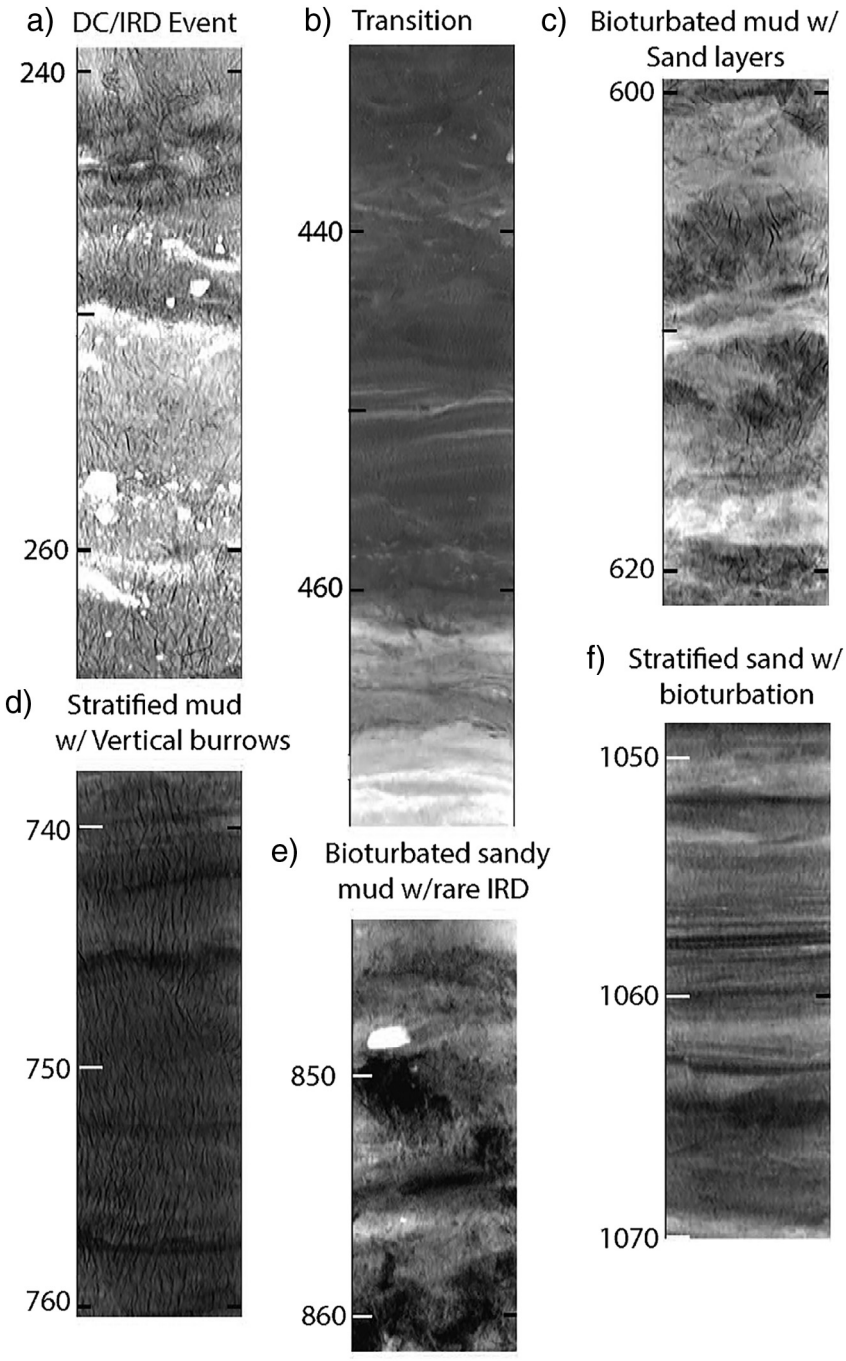

Fig. 4. Examples of lithofacies and bioturbation types from 2008029-12PC CT scans. See Fig. 3 for locations of these examples on the CT image of the core.

sheet grounding line was at or near the shelf edge, has higher magnetic susceptibility (Fig. 3C), variable sand content including high weight percentage peaks (Fig. 3D) and a west Greenlandic sediment composition (Fig. 3E) but rare > 2 mm clasts (Fig. 3B). From the base of the core to 1022 cm, sediments are laminated mud with straight, sharp contacts defining the laminae and vertically oriented burrows (Fig. 4f). Between 1025 and 768 cm the sand content increases and stratification is disrupted by bioturbation (Fig. 3E). Stratified mud with distinct vertical burrows extends from 768 to 735 cm (Fig. 3D). From 735 cm to 688 cm sand content increases. This sandy unit is overlain by another sequence of stratified mud with distinct burrows between 688 and 630 cm. The sediment between 630 and 467 cm is bioturbated, stratified mud with layering disturbed by bioturbation (Fig. 4c). The uppermost part of this unit has high sand content and marks the transition to the upper lithofacies unit.

The upper lithofacies from 467 to 0 cm, which represents deglaciation and the Holocene (Jennings et al., 2017), has overall lower CT number (lower density) (Fig. 3A), lower magnetic susceptibility (Fig. 3C) and generally lower sand content (Fig. 3D). But, it has much higher numbers of > 2 mm clasts (IRD) (Fig. 3B). Immediately above the boundary the sediments are low-density bioturbated mud with the sand fraction comprising *Coscinodiscus* planktic diatoms and setae of *Chaetoceras*, consistent with the low MS values (Fig. 3c). Well-defined, thin laminae and rare IRD occur at the base of the unit, but transition upward to less-well defined laminae and rare to absent IRD from 420 cm to 352 cm. This fine interval was interpreted to record a period in the initial deglaciation as the grounding line retreated off the shelf edge with retention of an ice shelf (Jennings et al., 2017). At 352 cm (marked by middle horizontal blue line on Fig. 3) the CT # (density), MS and sand increase (Fig. 3A, B, C, D). This level marks the start of

renewed retreat of the GIS grounding line by calving (Jennings et al., 2017). The sediments are bioturbated but stratification is still evident, suggesting moderate sedimentation rates. Apart from a peak in > 2 mm clasts of west Greenland provenance at 330 cm the main rise in > 2 mm clasts coincides with the entry of the Northern Baffin Bay sediment source (NBB source) at 290 cm (Fig. 3B, E). Bioturbated, pebbly mud associated with a rise in NBB provenance occurs between 280 and 175 cm with the highest IRD interval from 280 to 240 cm (Fig. 3B, E). This NBB DC interval has been found in several cores on the central West Greenland slope (Sheldon et al., 2016; Jennings et al., 2017; Jackson et al., 2017) and has been correlated to BBDC1 (Simon et al., 2012, 2014; Jackson et al., 2017), marking the retreat of NBB ice streams. The NBB DC event is overlain by bioturbated mud with small, dispersed IRD and discontinuous silt stringers between 175 and 152 cm. Bioturbated pebbly mud between 152 and 52 cm has high NBB provenance between 160 and 90 cm, an interval that contains an age reversal and a mixture of radiocarbon ages (Fig. 3F). The age reversal suggests that the upper NBB peak is reworked. The upper 52 cm of the core is bioturbated mud with dispersed IRD likely represents the middle to late Holocene time period, although it is undated.

4.2. Biological proxies

Biological proxy data are expressed against age using the age model based on ΔR = 140 yrs. (Fig. 5).

4.2.1. Bioturbation

The CT scan image (Fig. 3) reveals that the entire core is bioturbated, indicating that there was sufficient oxygenation and food to support the benthos in Baffin Bay throughout the time period represented by the core (Löwemark et al., 2012). Variations in burrow shape and density are indicative of the interplay between oxygenation, sedimentation rate, sedimentation processes, substrate consistency and food supply (Reineck and Singh, 1980; Wetzel, 1991; Löwemark et al., 2012) (Fig. 4). Intensely bioturbated intervals in which sand layers are disrupted by burrowing (e.g. Fig. 4a, c, e) suggest periods of relatively slow sedimentation (Wetzel, 1991), whereas intervals of vertical burrows terminated by overlying strata (e.g. Fig. 4d, f) indicate episodic rapid sedimentation (Jennings et al., 2011). Fig. 4 shows expanded views of segments of the CT image shown in full on Fig. 3 to illustrate some of the key lithofacies characteristics and trace fossil types that provide evidence for sedimentation processes. Muddy intervals typically have vertical burrows that are truncated by subsequent strata (Fig. 4d). These mud intervals likely represent plumites deposited from turbid meltwater plumes, whereas the sandy, stratified intervals with varying degrees of bioturbation likely represent distal turbidites (Ó Cofaigh and Dowdeswell, 2001) (Fig. 4c, f).

4.2.2. Foraminifera and stable isotopes

The Foraminiferal abundances in 12PC are spiky, with intervals of low benthic and planktic numbers per gram of dry sediment punctuated by periods of much higher numbers of foraminifers per gram (Fig. 5D). The high variability in abundance relates to variations in marine productivity, overprinted by carbonate dissolution, and dilution by high (12.8 cm/ka on average from 250 to 860 cm) and varying sedimentation rates. The lithofacies characteristics suggest widely varying sedimentation rates in the core that are not captured by the less frequent age control. Therefore we did not attempt to calculate foraminiferal flux, which would have been a more direct measure of productivity, but rather rely on foraminiferal numbers per gram as a measure of productivity.

N. pachyderma, the only planktic species, forms abundance spikes up to 1620 specimens/g, with intervening periods of very low abundance to absence (Fig. 5). The planktic forams were quite small from the base of the core to 860 cm (22 cal ka BP), but increased in size above that level. In general the planktic and benthic foram abundances rise and fall together, suggesting that the abundance spikes represent in situ productivity and a link between surface productivity and benthic food

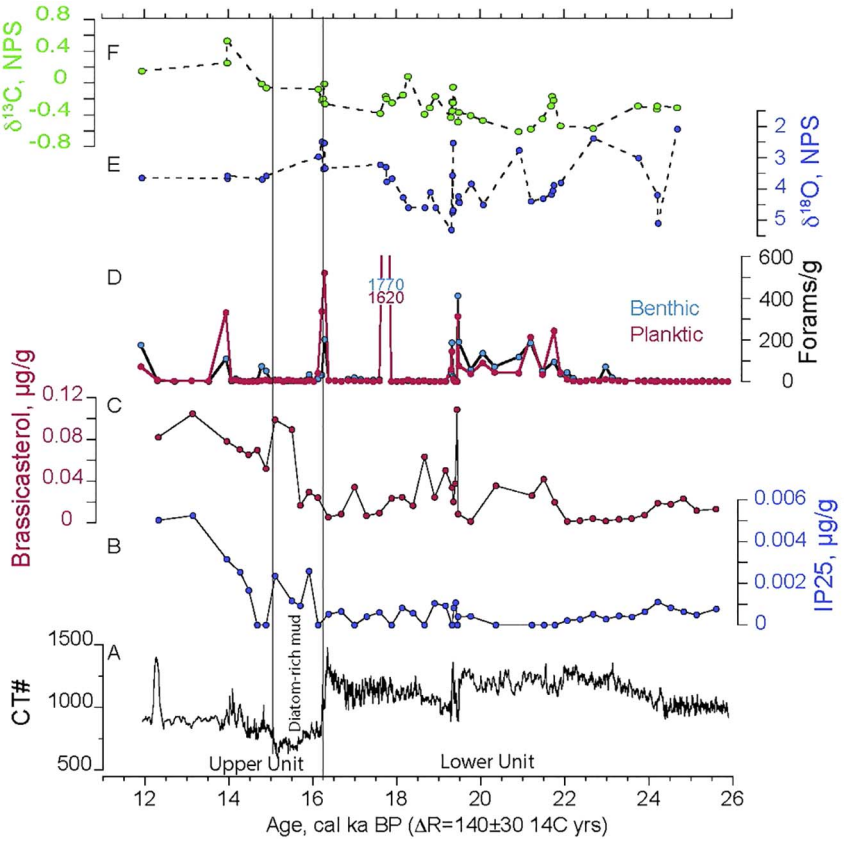

Fig. 5. Biological proxies from 12PC compared with CT# plot to assist with comparison to depth on depth in Fig. 3. A. CT#; B. sea ice biomarker, IP_{25}; C. marine productivity biomarker, brassicasterol; D. Benthic (blue) and planktic (red) forams per gram of dry sediment; E. $\delta^{18}O$ of planktic foraminifer, *N. pachyderma*, blue; F. $\delta^{13}C$ of *N. pachyderma*, green. (For interpretation of the references to colour in this figure legend, the reader is referred to the web version of this article.)

supply, although we cannot control for variations in carbonate preservation. Low numbers of *N. pachyderma* per gram are consistent with low productivity under perennial sea ice and the high numbers per gram are consistent with periods of more open water, such as leads or polynyas in summer (e.g. Nørgaard-Pedersen et al., 2003). Advection of planktic foraminifers from outside Baffin Bay is unlikely, especially given the linkage between the benthic and planktic productivity (cf Knutz et al., 2011; Nørgaard-Pedersen et al., 2003).

Oxygen isotope values on *N. pachyderma* ranged between 5.4 and 2‰. The interval between 22 and 18.2 cal ka BP has mostly heavy values that fall between 4 and 5‰ (Fig. 5), comparable to MIS 2 values in the Fram Strait (Nørgaard-Pedersen et al., 2003). A shift to lighter $\delta^{18}O$ and $\delta^{13}C$ values begins at 18 cal ka BP, suggests reduced ventilation (Sarnthein et al., 1995). This interval falls within HS1 regardless of which ΔR is applied (Fig. 2; Table 1). Above this shift the $\delta^{18}O$ values remain above 3.7‰. A pronounced light $\delta^{18}O$ spike at 19.4 cal ka BP corresponds to high planktic abundance and increased IP_{25} and Brassicasterol (Fig. 5). Oxygen isotopic values of this magnitude can either be related to glacial meltwater, especially if they are paired with light $\delta^{13}C$ values (Sarnthein et al., 1995) or to increased rate of sea-ice production that can produce brines with a light isotopic signature (Hillaire-Marcel et al., 1989; Hillaire-Marcel and de Vernal, 2008). The overall trend in the $\delta^{13}C$ values is toward heavier values suggesting better ventilation at the top of the record than at the bottom (Fig. 5).

The benthic foraminiferal assemblages (Fig. 6) provide insights into the productivity of surface waters, stratification of the water column, and turbid glacial meltwater influx. For example, sea-ice edge migration, either seasonal or in the form of leads or polynyas, produces pulses of phytoplankton production that sink to the seabed, providing food for benthic communities. The three most common benthic foraminiferal species in 12PC are *Stainforthia feylingi*, *Cassidulina reniforme* and *Elphidium excavatum* forma *clavata*. *S. feylingi* is dominant in conditions of stratified water column with a cold freshwater lid and has been associated with productivity at the seasonal sea ice edge (Seidenkrantz, 2013). It has been found in high abundances associated with biosiliceous sediments (Jennings et al., 2006). *E. excavatum* and *C. reniforme* occur together in glacial marine settings (Hald and Korsun, 1997). *C. reniforme* is also considered to represent chilled Atlantic Water (Slubowska et al., 2005) and is found in areas of relatively high, stable salinities (Polyak et al., 2002). *E. excavatum* is an opportunistic species that thrives in unstable environmental conditions influenced by rapid sedimentation and fluctuating salinities from turbid meltwater plumes (Hald and Korsun, 1997). The agglutinated species, *Spiroplectammina biformis*, which occurs mainly in the lower lithofacies unit is found in arctic fjords with strong meltwater signal (Jennings and Helgadottir, 1994; Schafer and Cole, 1988).

Several species indicative of marine productivity associated with nutrient rich Atlantic Water occur in both the lower and upper lithofacies unit: *Melonis barleeanus*, *Buccella frigida*, *Nonionella turgida* and *Nonionellina labradorica*. *Islandiella norcrossi* and *I. helenae* both are arctic species, but *I. helenae* is associated with sea-ice edge productivity while *I. norcrossi* reflects chilled Atlantic Water of normal marine salinity (Polyak et al., 2002; Wollenburg et al., 2004; Lloyd, 2006). *I. norcrossi* is a common calcareous species on the west Greenland shelf associated with Atlantic Water in the West Greenland Current (e.g. Lloyd, 2006; Perner et al., 2012).

Near the top of the lower unit (16.5 cal ka BP), and continuing into the base of the overlying biosiliceous mud, several species associated with marine productivity and nutrient rich Atlantic Water spike to high percentages. These include *N. turgida*, *M. barleeanus*, *B. frigida*, *I. norcrossi* and very low percentage of *Pullenia bulloides*. Current indicator species, *Cibicides lobatulus* also increases at this boundary. The central part of the diatom-rich mud is barren of calcareous foraminifers and is characterized by low faunal abundances dominated by agglutinated foraminiferal species (e.g. *Textularia earlandi*), suggesting that dissolution of carbonate likely overprinted the assemblages. The upper part of

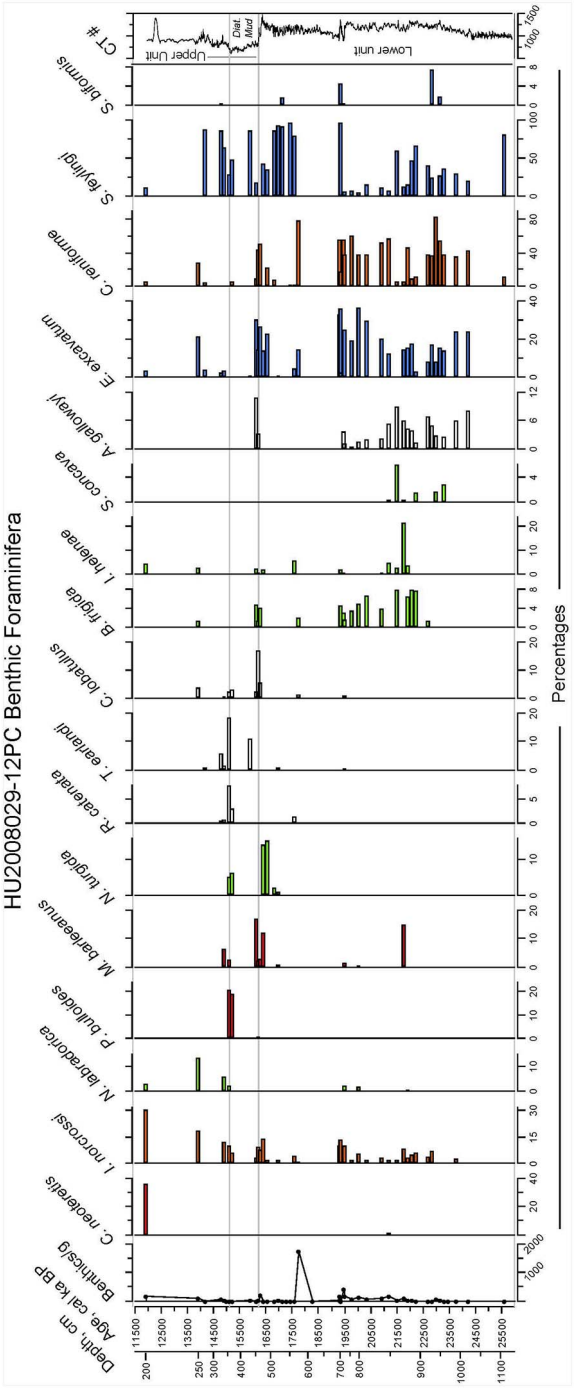

Fig. 6. Benthic foraminiferal species in 12PC. Green represent marine productivity species; red = Atlantic Water species; blue = Arctic species; light blue; Glacial marine species; orange = transformed (cooler and slightly lower salinity) Atlantic Water species. (For interpretation of the references to colour in this figure legend, the reader is referred to the web version of this article.)

the diatom-rich mud shows a return of several of the marine productivity species along with increased percentages of *P. bulloides*, a chilled Atlantic water species, that is common on the SE Greenland and Northern Iceland shelves under conditions of strong Irminger Current Atlantic water inflow (Eiríksson et al., 2000; Jennings et al., 2011).

Above the diatom-rich mud, the percentages of *N. labradorica* and *I. norcrossi* increase, and *S. feylingi* continues with high percentages. The chilled Atlantic Water species, *Cassidulina neoteretis*, is abundant at the top of the dated section along with *I. norcrossi*, consistent with intermediate Atlantic Water and less prominent glacial meltwater influence (Jennings and Helgadottir, 1994). The gap in foraminifers between 12 and 13.9 cal ka BP is likely a consequence of carbonate dissolution as other cores from the central West Greenland margin, but in slightly shallower water (JR175-VC29; Fig. 1) have *C. neoteretis* continuously between 14 and 11 cal ka BP (Jennings et al., 2017).

4.2.3. Biomarkers

Further evidence of marine productivity and sea ice comes from the algal biomarkers brassicasterol and IP_{25} (Fig. 5). In general, the presence of IP_{25} indicates release from melting seasonal sea ice (Fahl and Stein, 2012; Belt et al., 2013), while the absence of IP_{25} is consistent with intervals of thick perennial sea ice cover or no ice cover at all (Fahl and Stein, 2012). Brassicasterol implies productivity in open-water conditions, but it also can come from melting sea ice (Belt et al., 2013). In addition, the occurrence of polynyas has been given as a possible reason for presence of IP_{25} and brassicasterol under otherwise heavy ice conditions, even in the central Arctic Ocean (Xiao et al., 2013).

In the lower, high CT lithofacies unit of 12PC, brassicasterol and IP_{25} are present in low abundances from 26 to 22 ka (ΔR = 140 yrs), coinciding with low foraminiferal abundances (Fig. 5). Between 22 and 20 ka, brassicasterol rises but IP_{25} is low to absent. Foraminiferal abundances rise in this interval and the benthic fauna is characterized by productivity species (*B. frigida*, *I. helenae*, *M. barleeanus* and *N. labradorica*). An overall rise in IP_{25} and a large peak in brassicasterol occur at 19.5 ka, and continue with moderate values until another rise in brassicasterol values within the diatom-rich mud unit (16.2 to 15.1 cal ka BP). Both IP_{25} and brassicasterol continue to rise after 15.1 cal ka BP, but IP_{25} in particular rises to values unprecedented in the core after 14.3 cal ka BP.

This pattern of presence of IP_{25} and brassicasterol in the lower lithofacies unit argues for seasonal sea ice and some open water, although the generally low concentrations suggest that these were both likely less than in the upper unit - probably due to more extensive ice cover and only periodic opening - possibly as leads or polynyas. As the final increase in IP_{25} beginning at 16.2 ka is accompanied by rising, high brassicasterol it likely points to development of a marginal ice zone where there is increased marine productivity with probably more seasonal sea ice presence than before.

5. Discussion

5.1. Did an LGM Ice Shelf cover Baffin Bay?

There has been limited research on the LGM within Baffin Bay, which explains how the Baffin Bay ice shelf concept has remained untested. Radiocarbon dates on planktic foraminifers indicate that other cores besides 12PC have planktic fauna in the LGM. Andrews et al. (1998) obtained a pair of AMS ^{14}C dates from abundant planktic foraminifera in southern Baffin Bay core HU77029-017PC (17,990 ± 110, and 17,930 ± 210 ^{14}C yrs.; Andrews et al., 1998) (Fig. 1). These ^{14}C ages calibrate to the LGM (~21 ka BP; ΔR = 140 years). A ^{14}C date on planktic foraminifers from core HE006–4-2PC (21,440 ± 140 ^{14}C yrs) on the northern side of the Uummannaq TMF (Fig. 1) calibrates to ~25 ka BP (ΔR = 140 years) (Ó Cofaigh et al., 2013a). In the LGM interval of 12PC (1130 cm to at least 690 cm) when the modeled Baffin Bay ice shelf would be in place, there are multiple lines of evidence for biological activity, including bioturbation, algal biomarkers and benthic and planktic foraminifers (Figs. 3–6). These findings are consistent with perennial sea-ice cover with some open water in the form of leads or polynyas on the eastern side of Baffin Bay. Full ice-shelf cover from an ice shelf extending from the Hudson Strait ice stream and grounding on Davis Strait all the way to Greenland (Álvarez-Solas et al., 2010, 2011; Marcott et al., 2011) would not allow the surface productivity (e.g. algal biomarkers, planktic forams) in Baffin Bay that would be needed to feed the benthic organisms that are evident (bioturbation and benthic foraminifers). On this basis we reject the modeling result of a full Baffin Bay ice shelf. While life has been observed under modern ice shelves in Antarctica, it is dependent on strong ocean inflow to the sub ice-shelf cavity from outside the ice shelf (Post et al., 2014). In the case of the Baffin Bay ice shelf cover as it is modeled, it would be sealed from the Labrador Sea marine advection and food supply.

The idea of the Davis Strait grounded ice shelf sprang in part from efforts to test a mechanism for Heinrich Event 1 (H1), in which subsurface warming reconstructed in the N. Atlantic in response to reduced Atlantic meridional overturning circulation (AMOC) during HS1 (McManus et al., 2004) weakens a buttressing ice shelf fronting the Hudson Strait ice stream and produces a Heinrich event (Álvarez-Solas et al., 2010, 2011; Marcott et al., 2011). Hulbe et al. (2004) modified their original 1997 Labrador Sea ice shelf idea to support instead fringing ice shelves along the coasts in Eastern Canada that were proposed to have met their demise through a process of meltwater infilling of surface crevasses. The existence of this type of ice shelf and H-event process has been contested (Alley et al., 2005), but it is more consistent with the 12PC data than the original idea of an ice shelf grounding on Davis Strait (Hulbe, 1997).

5.2. Heinrich Stadial environments

The data in 12PC allow examination of the environmental response in Baffin Bay to the transition from LGM to HS1, and the response in Baffin Bay to the large ice discharge from Hudson Strait during H1 which occurred when subsurface ocean heat was at a maximum and AMOC at a minimum (Marcott et al., 2011). Locating the LGM/HS1 transition and H1 in 12PC is made difficult by the uncertainties in the magnitude of the local marine reservoir age through time (Fig. 3F) (Stern and Lisiecki, 2013). The accepted timing of H1 calving event is 16.8 ka BP (Hemming, 2004), although it may be closer to 16 ka BP based on the timing of the peak of IRD in the North Atlantic IRD stack during HS1 (Stern and Lisiecki, 2013). If we apply the ΔR envelope approach using data from Stern and Lisiecki (2013) to the mean value of the best 2 constraining radiocarbon ages from the base of DC1 (= H1) in cores HU75009-IV-055PC and HU87033-009 LCF (Fig. 1; Andrews et al., 1994; Jennings et al., 1996), from the Labrador Sea, we obtain a range of ages for the event that spans HS1 (Table 1). The ΔR that matches best the H1 16.8 ka age determined by Hemming (2004) is the lower ΔR from Stern and Lisiecki (2013) (Table 1). On this basis, we chose to use the Lower ΔR to determine where HS1 lies in the 12PC record. Lower ΔR places the base of HS1 (18 ka BP) at 610 cm and its end (14.7 ka BP) at 395 cm, right at the end of the diatom-rich mud unit and before the initiation of calving retreat (Figs. 3F and 7). Lower ΔR also puts the calving retreat and the timing of the west Greenland DC event (= BBDC1; Jackson et al., 2017) (Fig. 3) in the Bølling/Allerød interstadial (Fig. 7). The age model calculated with an invariant ΔR = 140 years places the lithofacies transition which represents the grounding line retreat from the west Greenland shelf edge at 16.2 cal ka BP, within HS1 (Jennings et al., 2017), but places the end of HS1 after the initiation of GIS calving retreat.

Fig. 7 illustrates how key proxy data map into the Heinrich Stadial interval defined by evidence of sluggish AMOC (McManus et al., 2004) using the lower ΔR of Stern and Lisiecki (2013). In the Labrador Sea HS1 is an interval of anomalously warm bottom waters (Marcott et al.,

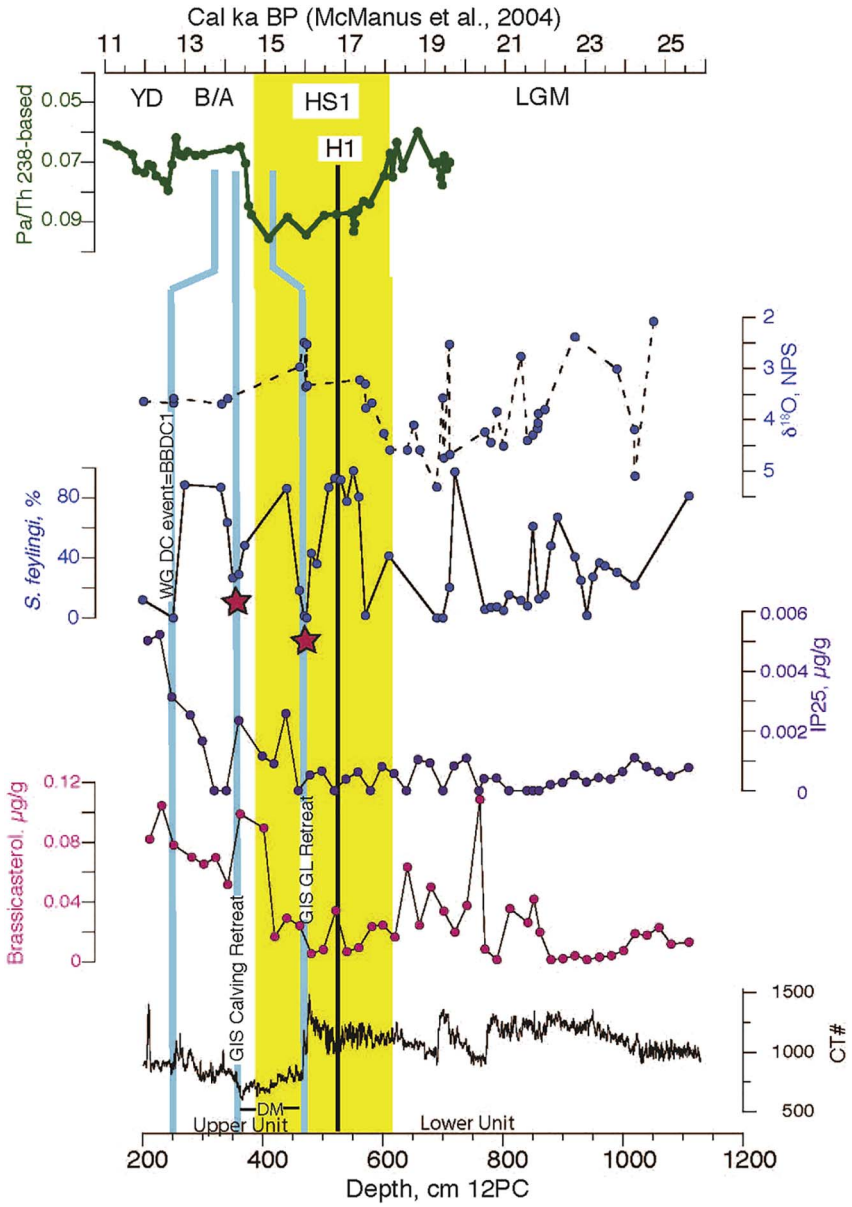

Fig. 7. Comparison between Pa/Th record of AMOC (McManus et al., 2004) and the timing of Heinrich Event 1 (H1) to key paleoenvironmental proxies in 12PC. The HS1 interval (yellow box) is defined in the core with use of the Lower ΔR of Stern and Lisiecki (2013) (Fig. 3f). Blue lines show where key events in the core map into the climatic intervals with use of the Lower ΔR of Stern and Lisiecki (2013). A. CT # from 12PC; B. Brassicasterol, 12PC; C. IP_{25}, 12PC; D. *Stainforthia feylingi*, 12PC; E. Oxygen isotope ratios, 12PC; F. Pa/Th ratios (McManus et al., 2004). (For interpretation of the references to colour in this figure legend, the reader is referred to the web version of this article.)

2011) within which H1 occurred (Fig. 7). We would expect this massive freshwater (meltwater and icebergs) outflow from collapse of the Hudson Strait ice stream (Andrews and Tedesco, 1992; Hesse and Khodabakhsh, 2016) to perturb environments in Baffin Bay or initiate a transition to different paleoceanographic conditions.

The transition to lighter $\delta^{18}O$ values and a shift to very high percentages of *S. feylingi* coincide with HS1 (Fig. 7). This signal is also seen in nearby core JR175-VC29 (Fig. 1), from 900 m water depth (Jennings et al., 2017) and is associated in both 12PC and VC29 with deposition of diatom-rich mud with rare IRD; a fine-grained unit of similar age is observed in core GeoTü SL-170 (Jackson et al., 2017) slightly north of VC29. The diatom-rich mud interval has been interpreted by Jennings et al. (2017) to indicate exclusion of coarse sediment delivery to the Disko TMF by retention of a fringing ice shelf after initial grounding line retreat. Overall, brassicasterol abundances are low in HS1. A period of high productivity of benthic forams indicative of nutrient rich Atlantic water at the subsurface (Fig. 5) (indicated on Fig. 7 by red stars and low percentages of the benthic foraminiferal species, *S. feylingi*) coincides with the initial GIS retreat from the shelf edge as indicated in the CT# profile (Jennings et al., 2017). Subsequent interstadial conditions are marked by rising marine productivity, renewed subsurface Atlantic Water influence, and renewed retreat of the GIS, followed by development of consistent seasonal sea ice and release/melting of detrital carbonate bearing ice bergs from ice margins of northern Baffin Bay termed a west Greenland DC event by (Jennings et al., 2017) that has been shown to be correlative to BBDC1 (Simon et al., 2016 by Jackson et al. (2017).

6. Conclusions

1. Based on the data presented we reject the hypothesis that Baffin Bay was covered by a full ice shelf during the LGM. We conclude instead that Baffin Bay was perennially sea-ice covered with nutrient rich, relatively warm Atlantic water present at depth through the LGM. Evidence of marine productivity suggests that there were openings in the sea-ice cover as leads and polynyas to support marine productivity. Concurrently, sediment-laden, glacial-meltwater and turbidity currents were released from the GIS, grounded at the shelf edge, but IRD was rare suggesting the ice front was protected by a fringing ice shelf and/or the perennial sea-ice cover.
2. Reduced ventilation and productivity, coincident with a cold surface lid of meltwater was established in HS1. After Heinrich Event 1, but

within the Heinrich Stadial, an interval of increased productivity and Atlantic Water is associated with the retreat of the GIS grounding line from the shelf edge.
3. The implication for Heinrich Events and Ocean warming/Ice Shelf hypothesis is that perennial sea-ice cover and/or fringing ice shelves may be sufficient to explain the heat retention and back-pressure proposed to explain the dynamics that produce Heinrich Events.

Acknowledgements

Funding for this research was provided by the US National Science Foundation grant ARC1203492 and the UK Natural Environment Research Council grant NE/D001951/1. We thank the captain, crew and scientists aboard the 2008 CSS Hudson cruise HU2008-029 for acquisition of core 2009029-12PC. We gratefully acknowledge the microscope and X-ray diffraction research by undergraduate research assistants, Brian Shreve, Jennifer Kelly, Matthew Reed, and Matthew Glasset. We thank Quentin Simon and one anonymous reviewer for helpful critique of the manuscript.

References

Aksu, A.E., 1985. Climatic and oceanographic changes over the past 400,000 years: evidence from deep-sea cores on Baffin Bay and David Strait. In: Andrews, J.T. (Ed.), Quaternary Environments: Eastern Canadian Arctic, Baffin Bay and Western Greenland. Allen and Unwin, Boston, pp. 181–209.

Alley, R.B., Andrews, J.T., Barber, D.C., Clark, P.U., 2005. Comment on "catastrophic ice shelf breakup as the source of Heinrich event icebergs" by C.L. Hulbe et al. Palaeoceanography 20 (doi:10:1029/2004PA001086).

Álvarez-Solas, J., Charbit, S., Ritz, C., Paillard, D., Ramstein, G., Dumas, C., 2010. Links between ocean temperature and iceberg discharge during Heinrich events. Nat. Geosci. 3, 122–126.

Álvarez-Solas, J., Montoya, M., Ritz, C., Ramstein, G., Charbit, S., Dumas, C., Nisancioglu, K., Dokken, T., Ganopolski, A., 2011. Heinrich event 1: an example of dynamical ice-sheet reaction to ocean changes. Clim. Past 7, 1297–1306. http://dx.doi.org/10.5194/cp-7-1297-2011.

Andrews, J.T., Eberl, D.D., 2011. Surface (sea floor) and near-surface (box cores) sediment mineralogy in Baffin Bay as a key to sediment provenance and ice sheet variations. Can. J. Earth Sci. 48 (9), 1307–1328. http://dx.doi.org/10.1139/-11-021.

Andrews, J.T., Eberl, D.D., 2012. Determination of sediment provenance by unmixing the mineralogy of source-area sediments: the "SedUnMix" program. Mar. Geol. 291, 24–33.

Andrews, J.T., Erlenkeuser, H., Tedesco, K., Aksu, A., Jull, A.J.T., 1994. Late quaternary (stage 2 and 3) meltwater and Heinrich events, NW Labrador Sea. Quat. Res. 41, 26–34.

Andrews, J.T., Gibb, O.T., Jennings, A.E., Simon, Q., 2014. Variations in the provenance of sediment from ice sheets surrounding Baffin Bay during MIS 2 and 3 and export to the Labrador Shelf Sea: site HU2008029-0008 Davis Strait. J. Quat. Sci. 29, 3–13.

Andrews, J.T., Kirby, M.E., Aksu, A., Barber, D.C., Meese, D., 1998. Late quaternary detrital carbonate (DC-) events in Baffin Bay (67°–74° N): do they correlate with and contribute to Heinrich events in the North Atlantic? Quat. Sci. Rev. 17, 1125–1137.

Andrews, J.T., Tedesco, K., 1992. Detrital carbonate-rich sediments, northwestern Labrador Sea: implications for ice-sheet dynamics and iceberg rafting (Heinrich) events in the North Atlantic. Geology 20, 1087–1090.

Belt, S.T., Brown, T.A., Navarro Rodriguez, A., Cabedo Sanz, P., Tonkin, A., Ingle, R., 2012. A reproducible method for the extraction, identification and quantification of the Arctic sea ice proxy IP25 from marine sediments. Anal. Methods 4, 705–713.

Belt, S.T., Brown, T.A., Ringrose, A.E., Cabedo-Sanz, P., Mundy, C.J., Gosselin, M., Poulin, M., 2013. Quantitative measurement of the sea ice diatom biomarker IP25 and sterols in Arctic sea ice and underlying sediments: further considerations for palaeo sea ice reconstrucion. Org. Geochem. 62, 33–45.

Belt, S.T., Cabedo-Sanz, P., Smik, L., Navarro-Rodriguez, A., Berben, S.M., Knies, J., Husum, K., 2015. Identification of paleo Arctic winter sea ice limits and the marginal ice zone: optimised biomarker-based reconstructions of late quaternary Arctic sea ice. Earth Planet. Sci. Lett. 431, 127–139.

Blake Jr., W., 1977. Glacial sculpture along the east-central coast of Ellesmere Island, Arctic Archipelago. In: Current Research, Part C, Geological Survey of Canada, Paper 77-1C. 107–115.

Briner, J.P., Miller, G.H., Davis, P.T., Bierman, P.R., Cafee, M., 2003. Last glacial maximum ice sheet dynamics in Arctic Canada inferred from young erratics perched on ancient tors. Quat. Sci. Rev. 22, 437–444.

Brown, T.A., Belt, S.T., 2012. Closely linked sea ice–pelagic coupling in the Amundsen Gulf revealed by the sea ice diatom biomarker IP25. J. Plankton Res. 34, 647–654.

Buch, E., 2000a. A monograph on the physical oceanography of the Greenland waters. In: Danish Meteorological Institute Scientific Report, pp. 00–12.

Buch, E., 2000b. Air-sea-ice conditions off southwest Greenland, 1981–1997. J. Northwest Atl. Fish. Sci. 26, 1–14.

Buizert, C., Gkinis, V., Severinghaus, J.P., He, F., Lecavalier, B.S., Kindler, P., Leuenberger, M., Carlson, A.E., Vinther, B., Masson-Delmotte, V., White, J.W.C., Liu, Z., Otto-Bliesner, B., Brook, E.J., 2014. Greenland temperature response to climate forcing during the last deglaciation. Science 345, 1177–1180. http://dx.doi.org/10.1126/science.1254961.

Campbell, D.C., de Vernal, A., 2009. CCGS Hudson expedition 2008029: marine geology and paleoceanography of Baffin Bay and adjacent areas, Nain, NL to Halifax, NS, August 28–September 23. In: Geological Survey of Canada, Open File 5989, 2009, http://dx.doi.org/10.4095/261330. (212 pages; 1 DVD).

Clark, P.U., Dyke, A.S., Shakun, D., Carlson, A.E., Clark, J., Wohlfarth, B., Mitrovica, J.X., Hostetler, S.W., McCabe, A.M., 2009. The last glacial maximum. Science 325, 710–714.

Dahl-Jensen, D., Al, E., 1998. Past temperatures directly from the Greenland ice sheet. Science 282, 268–271.

Darling, K.F., Kucera, M., Kroon, D., Wade, C.M., 2006. A resolution for the coiling direction paradox in *Neogloboquadrina pachyderma*. Paleoceanography 21, PA2011. http://dx.doi.org/10.1029/2005PA001189.

de Vernal, A., Bilodeau, G., Hillair-Marcel, C., Kassou, N., 1992. Quantitative assessment of carbonate dissolution in marine sediments from foraminifer linings vs. shell ratios: example from Davis Strait, NW North Atlantic. Geology 20, 527–530.

Domack, E.W., Harris, P.T., 1998. A new depositional model for ice shelves, based upon sediment cores from the Ross Sea and the Mac. Roberson shelf, Antarctica. Ann. Glaciol. 27, 281–284.

Dowdeswell, J.A., Hogan, K.A., Ó Cofaigh, C., Fugelli, E.M.G., Evans, J., Noormets, R., 2014. Late quaternary ice flow in a West Greenland fjord and cross-shelf trough system: submarine landforms from Rink Isbrae to Uummannaq shelf and slope. Quat. Sci. Rev. 92, 292–309. http://dx.doi.org/10.1016/j.quascirev.2013.09.007.

Dyke, A.S., Andrews, J.T., Clark, P.U., England, J.H., Miller, G.H., Shaw, J., Veillette, J.J., 2002. The Laurentide and Innuitian ice sheets during the last glacial maximum. Quat. Sci. Rev. 21, 9–31.

Eberl, D.D., 2003. User guide to RockJock: a program for determining quantitative mineralogy from X-ray diffraction data. In: United States Geological Survey, Open File Report 03–78, Washington, DC, (40 pp).

Eiríksson, J., Knudsen, K.L., Haflidason, H., Henriksen, P., 2000. Late-glacial and Holocene palaeoceanography of the north Icelandic shelf. J. Quat. Sci. 15, 23–42.

England, J., 1999. Coalescent Greenland and Innuitian ice during the last glacial maximum: revising the quaternary of the Canadian high Arctic. Quat. Sci. Rev. 18, 421–426. http://dx.doi.org/10.1016/S0277-3791(98)00070-5.

England, J., Atkinson, N., Bednarski, J., Dyke, A.S., Hodgson, D.A., Ó Cofaigh, C., 2006. The Innuitian ice sheet: configuration, dynamics and chronology. Quat. Sci. Rev. 25, 689–703.

Fahl, K., Stein, R., 2012. Modern seasonal variability and deglacial/Holocene change of central Arctic Ocean sea ice cover: new insights from biomarker proxy records. Earth Planet. Sci. Lett. 351–352, 123–133.

Grobe, H., 1987. A simple method for the determination of ice-rafted debris in sediment cores. Polarforschung 57 (3), 123–126.

Hald, M., Korsun, S., 1997. Distribution of modern benthic foraminifera from fjords of Svalbard, European Arctic. J. Foraminifer. Res. 27, 101–122.

Hemming, S.R., 2004. Heinrich events: massive late Pleistocene detritus layers of the North Atlantic and their global climate imprint. Rev. Geophys. 42, RG1005.

Hesse, R., Khodabakhsh, S., 2016. Anatomy of Labrador Sea Heinrich layers. Mar. Geol. 380, 44–86. http://dx.doi.org/10.1016/j.margeo.2016.05.019.

Hesse, R., Khodabakhsh, S., Klaucke, I., Ryan, W.B.F., 1997. Asymmetrical turbid surface-plume deposition near ice-outlets of the Pleistocene Laurentide ice sheet in the Labrador Sea. Geo-Mar. Lett. 17, 179–187.

Hillaire-Marcel, C., de Vernal, A., 2008. Stable isotope clue to episodic sea-ice formation in the glacial North Atlantic. Earth Planet. Sci. Lett. 268, 143–150.

Hillaire-Marcel, C., de Vernal, A., Aksu, A.E., Macko, S., 1989. High-resolution isotopicand micropaleontological studies of upper Pleistocene sediments at ODP site 645, Baffin Bay. Proc. Ocean Drill. Program 105B, 599–616.

Hofmann, J.C., Knutz, P.C., Nielsen, T., Kuijpers, A., 2016. Seismic architecture and evolution of the Disko Bay trough-mouth fan, central West Greenland margin. Quat. Sci. Rev.. http://dx.doi.org/10.1016/j.quascirev.2016.05.019.

Hogan, K.A., Ó Cofaigh, C., Jennings, A.E., Dowdeswell, J.A., Hiemstra, J.F., 2016. Deglaciation of a major palaeo-ice stream in Disko Trough, West Greenland. Quat. Sci. Rev. http://dx.doi.org/10.1016/j.quascirev.2016.01.018.

Holland, D.M., Thomas, R.H., de Young, B., Ribergaard, M.H., Lyberth, B., 2008. Acceleration of Jakobshavn Isbræ triggered by warm subsurface oceanwaters. Nat. Geosci. 1 (10), 659e664. http://dx.doi.org/10.1038/ngeo316.

Hulbe, C.L., 1997. An ice shelf mechanism for Heinrich layer production. Paleoceanography 12, 711–717.

Hulbe, C.L., MacAyeal, D.R., Denton, G.H., Kleman, J., Lowell, T.V., 2004. Catastrophic ice shelf breakup as the source for Heinrich event icebergs. Palaeoceanography 19: 1 of 15http://dx.doi.org/10.1029/2003:PA000890. (002004).

Jackson, R., Carlson, A.E., Hillaire-Marcel, C., Wacker, L., Vogt, C., Kucera, M., 2017. Asynchronous instability of the North American-Arctic and Greenland ice sheets during the last deglaciation. Quat. Sci. Rev. 164, 140–153. http://dx.doi.org/10.1016/j.quascirev.2017.03.020.

Jennings, A.E., Andrews, J.T., Ó Cofaigh, C., St. Onge, G., Sheldon, C., Belt, S.T., Cabedo-Sanz, P., Hillaire-Marcel, C., 2017. Ocean forcing of ice sheet retreat in central West Greenland from LGM through deglaciation. Earth Planet. Sci. Lett. 472, 1–13.

Jennings, A.E., Andrews, J.T., Wilson, L., 2011. Holocene environmental evolution of the SE Greenland shelf north and south of the Denmark Strait: Irminger and East Greenland current interactions. Quat. Sci. Rev. 30, 980–998.

Jennings, A.E., Hald, M., Smith, L.M., Andrews, J.T., 2006. Freshwater forcing from the Greenland ice sheet during the Younger Dryas: evidence from southeastern Greenland shelf cores. Quat. Sci. Rev. 25, 282–298. http://dx.doi.org/10.1016/j.quascirev.2005.04.006.

Jennings, A.E., Helgadottir, G., 1994. Foraminiferal assemblages from the fjords and shelf of eastern Greenland. J. Foraminifer. Res. 24 (2), 123e144. http://dx.doi.org/10.2113/gsjfr.24.2.123.

Jennings, A.E., Sheldon, C., Cronin, T.M., Francus, F., Stoner, J., Andrews, J., 2011. The Holocene history of Nares Strait, transition from glacial bay to Arctic-Atlantic throughflow. Oceanography 24 (3), 26–41.

Jennings, A.E., Tedesco, K.A., Andrews, J.T., Kirby, M.E., 1996. Shelf erosion and glacial ice proximity in the Labrador Sea during and after Heinrich events (H-3 or 4 to H-0) as shown by foraminifera. In: Andrews, J.T., Austin, W.E.N., Bergsten, H., Jennings, A.E. (Eds.), Late Quaternary Palaeoceanography of the North Atlantic Margins. Geological Society Special Publications, pp. 29–49.

Jennings, A.E., Walton, M.E., Cofaigh, C.O., Kilfeather, A., Andrews, J.T., Ortiz, J.D., et al., 2014. Paleoenvironments during younger Dryas-early Holocene retreat of the Greenland ice sheet from outer Disko Trough, central west Greenland. J. Quat. Sci. 29 (1), 27e40. http://dx.doi.org/10.1002/jqs.2652.

Kaufman, D.S., Williams, K.M., 1992. Radiocarbon date list VII: Baffin Island, N.W.T., Canada. In: INSTAAR Occasional Paper 48. Institute of Arctic and Alpine Research, University of Colorado, Boulder (compilers).

Knudsen, K.L., Stabell, B., Seidenkrantz, M.-S., Eiríksson, J., Blake, W., 2008. Deglacial and Holocene conditions in northernmost Baffin Bay: sediments, foraminifera, diatoms and stable isotopes. Boreas 37 (3), 346–376. http://dx.doi.org/10.1111/j.1502-3885.2008.00035.x.

Knutz, P.C., Sicre, M.-A., Ebbesen, H., Christiansen, S., Kuijpers, A., 2011. Multiple-stage deglacial retreat of the southern Greenland ice sheet linked with Irminger current warm water transport. Paleoceanography 26, PA3204. http://dx.doi.org/10.1029/2010PA002053.

Li, G., Piper, D.J.W., Campbell, D.C., 2011. The quaternary Lancaster sound trough-mouth fan, NW Baffin Bay. J. Quat. Sci. 26, 511–522.

Lloyd, J.M., 2006. Modern distribution of benthic foraminifera from Disko Bugt, West Greenland. J. Foraminifer. Res. 36, 315–331.

Lloyd, J.M., Moros, M., Perner, K., Telford, R.J., Kuijpers, A., Jansen, E., et al., 2011. A 100 yr record of ocean temperature control on the stability of Jakobshavnlsbrae, West Greenland. Geology 39 (9), 867–870. http://dx.doi.org/10.1130/G32076.1.

Löwemark, L., O'Regan, M., Hanebuth, T.J.J., Jakobsson, M., 2012. Late quaternary spatial and temporal variability in Arctic deep-sea bioturbation and its relation to Mn cycles. Palaeogeogr. Palaeoclimatol. Palaeoecol. 365-366, 192–208.

Lucci, R.G., Rebesco, M., 2007. Glacial contourites on the Antarctic peninsula margin: insight for palaeoenvironmental and palaeoclimatic conditions. Geol. Soc. Lond., Spec. Publ. 276, 111–127.

Marcott, et al., 2011. Ice-shelf collapse from subsurface warming as a trigger for Heinrich events. In: PNAS 108. no. 33, pp. 13415–13419.

McManus, J.F., Francois, R., Gherardi, J.-M., Keigwin, L.D., Brown-Leger, S., 2004. Collapse and rapid resumption of the Atlantic meridional circulation linked to deglacial climate change. Nature 428, 834–837.

Münchow, A., Falkner, A., Melling, H., 2015. Baffin Island and West Greenland current systems in northern Baffin Bay. Prog. Oceanogr. 132, 305–317.

Nørgaard-Pedersen, N., Spielhagen, R.F., Erlenkeuser, H., Grootes, P.M., Heinemeier, J., Knies, J., 2003. Arctic Ocean during the last glacial maximum: Atlantic and polar domains of surface water mass distribution and ice cover. Paleoceanography 18, 2003. http://dx.doi.org/10.1029/2002PA000781.

Ó Cofaigh, C., Andrews, J.T., Jennings, A.E., Dowdeswell, J.A., Hogan, K.A., Kilfeather, A.A., et al., 2013a. Glacimarine lithofacies, provenance and depositional processes on a West Greenland trough-mouth fan. J. Quat. Sci. 28http://dx.doi.org/10.1002/jqs.2569. Available at:.

Ó Cofaigh, C., Dowdeswell, J.A., 2001. Laminated sediments in glacimarine environments: diagnostic criteria for their interpretation. Quat. Sci. Rev. 20, 1411–1436.

Ó Cofaigh, C., Dowdeswell, J.A., Jennings, A.E., Hogan, K.A., Kilfeather, A., Hiemstra, J.F., et al., 2013. An extensive and dynamic ice sheet on the West Greenland shelf during the last glacial cycle. Geology 41 (2), 219–222. http://dx.doi.org/10.1130/G33759.1.

Perner, K., Moros, M., Jennings, A., Lloyd, J.M., Knudsen, K.L., 2012. Holocene palaeoceanographic evolution off West Greenland. The Holocene 23, 374–387.

Piénkowski, A.J., England, J.H., Furze, M.F.A., Marret, F., Eynaud, F., Vilks, G., Maclean, B., Blasco, S., Scourse, J.D., 2012. The deglacial to postglacial marine environments of SEBarrow Strait, Canadian Arctic Archipelago. Boreas 41 (2), 141–179. http://dx.doi.org/10.1111/j.1502-3885.2011.00227.x.

Polyak, L., Korsun, S., Febo, L.A., Stanovoy, V., Khusid, T., Hald, M., Paulsen, B.E., Lubinski, D.J., 2002. Benthic foraminiferal assemblages from the southern Kara Sea, a river influenced Arctic marine environment. J. Foraminifer. Res. 32, 252–273.

Post, A.L., Galton-Fenzi, B.K., Riddle, M.J., Herraiz-Borreguero, L., O'Brien, P.E., Hemer, M.A., McMinn, A., Rasch, D., Craven, M., 2014. Modern sedimentation, circulation and life beneath the Amery ice shelf, East Antarctica. Cont. Shelf Res. 74, 77–87.

Ramsey, C.B., Lee, S., 2013. Recent and planned developments of the program OxCal. Radiocarbon 55, 720–730.

Reeh, N., Thomsen, H.H., Higgins, A.K., Weidick, A., 2001. Sea ice and the stability of north and northeast Greenland floating glaciers. In: Jeffries, M.O., Eicken, H. (Eds.), Annals of Glaciology. Vol. 33. pp. 474–480.

Reimer, P.J., Bard, E., Bayliss, A., Beck, J.W., Blackwell, P.G., Ramsey, C.B., Grootes, P.M., Guilderson, T.P., Haflidason, H., Hajdas, I., Hatté, C., Heaton, T.J., Hoffmann, D.L., Hogg, A.G., Hughen, K.A., Kaiser, K.F., Kromer, B., Manning, S.W., Niu, M., Reimer, R.W., Richards, D.A., Scott, E.M., Southon, J.R., Staff, R.A., Turney, C.S.M., van der Plicht, J., 2013. IntCal13 and Marine13 radiocarbon age calibration curves 0 − 50,000 years cal BP. Radiocarbon 55, 1869–1887. http://dx.doi.org/10.2458/azu_js_rc. (55.16947).

Reineck, H.E., Singh, I.B., 1980. Depositional Sedimentary Environments. Springer-Verlag, NY.

Sarnthein, M., et al., 1995. Variations in Atlantic surface ocean paleoceanography, 50_–80_N: a time-slice record of the last 30,000 years. Paleoceanography 10 (6), 1063–1094.

Schafer, C.T., Cole, F.E., 1988. Environmental associations of Baffin Island fjord agglutinated foraminifera. Abh. Geol. Bundesanst 307.

Seidenkrantz, M.-S., 2013. Benthic foraminifera as palaeo sea-ice indicators in the subarctic realm-examples from the Labrador Sea-Baffin Bay region. Quat. Sci. Rev. 79, 135–144. http://dx.doi.org/10.1016/j.quascirev.2013.03.014.

Sheldon, C., Jennings, A., Andrews, J.T., Ó Cofaigh, C., Hogan, K., Dowdeswell, J.A., Seidenkrantz, M.-S., 2016. Ice stream retreat following the LGM and onset of the west Greenland current in Uummannaq Trough, west Greenland. Quat. Sci. Rev. http://dx.doi.org/10.1016/j.quascirev.2016.01.019.

Simon, Q., Hillaire-Marcel, C., St-Onge, G., Andrews, J.T., 2014. Northeastern Laurentide, western Greenland and southern Innuitian ice stream dynamics during the last glacial cycle. J. Quat. Sci. 29 (1), 14–26. http://dx.doi.org/10.1002/jqs.2648.

Simon, Q., St-Onge, G., Hillaire-Marcel, C., 2012. Late Quaternary chronostratigraphic framework of deep Baffin Bay glaciomarine sediments from high-resolution paleomagnetic data. Geochem. Geophys. Geosyst. 13, Q0AO03. http://dx.doi.org/10.1029/2012GC004272.

Simon, Q., Thouveny, N., Bourles, D.L., Nuttin, L., Hillaire-Marcel, C., St-Onge, G., 2016. Authigenic $^{10}Be/^{9}Be$ ratios and ^{10}Be-fluxes ($^{230}Th_{xs}$-normalized) in central Baffin Bay sediments during the last glacial cycle: paleoenvironmental implications. Quat. Sci. Rev. 140, 142–162.

Slabon, P., Dorschel, B., Jokat, W., Myklebust, R., Hebbeln, D., Gebhardt, C., 2016. Greenland ice sheet retreat history in the northeast Baffin Bay based on high-resolution bathymetry. Quat. Sci. Rev. 154, 182–198. http://dx.doi.org/10.1016/j.quascirev.2016.10.022.

Slubowska, M.A., Koç, N., Rasmussen, T.L., Klitgaard-Kristensen, D., 2005. Changes in the flow of Atlantic water into the Arctic Ocean since the last deglaciation: evidence from the northern Svalbard continental margin, 80_N. Paleoceanography 20, PA4014. http://dx.doi.org/10.1029/2005PA001141.

Stern, J.V., Lisiecki, L.E., 2013. North Atlantic circulation and reservoir age changes over the past 41,000 years. Geophys. Res. Lett. 40, 3693–3697. http://dx.doi.org/10.1002/grl.50679.

Straneo, F., Sutherland, D.A., Holland, D., Gladish, C., Hamilton, G.S., Johnson, H.L., Rignot, E., Xu, Y., Koppes, M., 2012. Characteristics of ocean waters reaching Greenland's glaciers. Ann. Glaciol. 53 (60), 202–210. http://dx.doi.org/10.3189/2012AoG60A059.

Tang, C.C.L., Ross, C.K., Yao, T., Petrie, B., DeTracey, B.M., Dunlap, E., 2004. The circulation, water masses and sea-ice of Baffin Bay. Prog. Oceanogr. 63, 183–228.

Wetzel, A., 1991. Ecologic interpretation of deep-sea trace fossil co = unities. Palaeogeogr. Palaeoclimatol. Palaeoecol. 85, 47–69.

Wollenburg, J.E., Knies, J., Mackensen, A., 2004. High-resolution paleoproductivity fluctuations during the past 24 kyr as indicated by benthic foraminifera in the marginal Arctic Ocean. Palaeogeogr. Palaeoclimatol. Palaeoecol. 204, 209–238.

Xiao, X., Fahl, K., Stein, R., 2013. Biomarker distributions in surface sediments from the Kara and Laptev seas (Arctic Ocean): indicators for organic-carbon sources and sea ice coverage. Quat. Sci. Rev. 79, 40–52.

Zreda, M., England, J., Phillips, F., Elmore, D., Sharma, P., 1999. Unblocking of the Nares Strait by Greenland and Ellesmere ice-sheet retreat 10,000 years ago. Nature 398, 139–142. http://dx.doi.org/10.1038/18197.